Chalcogenide Letters Vol. 11, No. 7, July 2014, p. 337 - 349

SUBSTRATE TEMPERATURE AND FILM THICKNESS DEPENDENCE OF THE OPTICAL AND ELECTRICAL PROPERTIES OF AMORPHOUS $As_{46}Te_{46}S_8$ THIN FILMS

A.A. ABU-SEHLY[a], A.S. SOLTAN[a], A.A. JORAID[b]*
[a]*Physics Department, Faculty of Science, Assiut University, Assiut, Egypt*
[b]*Physics Department, Taibah University, Madinah, Saudi Arabia*

Thin films of $As_{46}Te_{46}S_8$ with different thicknesses were prepared via thermal evaporation onto chemically cleaned glass substrates at different temperatures. X-ray diffraction of the deposited film at room temperature revealed the formation of an amorphous structure. In addition, the selected-area electron diffraction (SAED) patterns confirmed the amorphous phase. The mechanism of the optical absorption was observed to follow the rule of direct transition. An increase in the optical gap (E_0) from 2.35 to 2.73 eV was observed when the substrate temperature T_S was varied from room temperature to 463 K (film thickness = 100 nm). In addition, E_0 was observed to be dependent on the film thickness and increased from 1.7 to 2.38 eV when the film thickness was increased from 35 to 135 nm (T_S = room temperature). The effect of T_S on the electrical properties was also studied. The electrical resistivity (ρ) and the activation energy for conduction (ΔE) decreased from 7.74 x10^5 to 6.81 x 10^2 Ω cm and from 0.55 to 0.15 eV, respectively, when T_S increased from room temperature to 448 K (film thickness = 100 nm). The Mott and Davis model for the density of states in amorphous solids was used to interpret and discuss the results.

(Received June 18, 2014; Accepted July 18, 2014)

Keywords: Chalcogenides; Substrate temperature; Optical constant; Morphology; Film thickness; Optical band gap; Dielectric constant; Absorption coefficient

1. Introduction

Thin films play a crucial role in science and technology due to their wide use in a large number of active and passive devices such as the target material of television cameras, microwave devices, switching devices and diodes [1, 2].

Due to their high optical transparency in the IR region, strong optical nonlinearity, high photosensitivity, ease of fabrication and processing, and good chemical durability, chalcogenide glasses based on the chalcogen elements S, Se, and Te are widely used in ultra-fast optical switches, frequency converters, optical amplifiers, optical recording devices, optical integrated circuits for IR operations and infrared transmitting optical fibres [3-7]. Arsenic chalcogenides have been investigated extensively [8-10]. Many studies in the literature [9-13] have reported various properties of amorphous alloys belonging to $A_x^V\ B_{1-x}^{VI}$ systems, where A is a group V element, such as As, and B is a group VI element, such as Te, Se, or S.

Chalcogenide glasses in general and vitreous Te-based alloys in particular have been the subject of extensive work, with an emphasis on structure change due to their new technological applications in optical data storage [14]. Moreover, tellurium alloys have often been used for the active layer of memory devices [15] because of their low melting points. The structural bonding of chalcogens, e.g., tellurium, is divalent in nature, which provides the one-dimensional structural stability of amorphous materials. The structural bonding in the amorphous matrix is not highly stable [15, 16], and chalcogens in the amorphous state have a strong tendency to crystallise.

*Corresponding author: aaljoraid@taibahu.edu.sa

Arsenic trisulphide (As_2S_3) has also been the subject of extensive studies due to its wide applications in infrared optics and optical coatings because of its excellent IR transmission, large glass forming tendency, and resistance to moisture and chemicals [17].

The effect of Te addition on the optical properties of As_2S_3 thin films has been reported [18]. The reduction of the optical band gap was due to the creation of localised states. New bonds were formed due to the photo diffusion of Te into the As_2S_3 matrix. The structural basis of As-Te was investigated by several researchers using X-ray scattering [19, 20] and Mossbauer studies [21].

There are various deposition parameters, such as thickness and substrate temperature, type of substrate and deposition rate, etc, on which properties of films may depend [1]. In the present work, the effect of substrate temperature on the optical band gap and the activation energy for conduction was studied for thermally evaporated $As_{46}Te_{46}S_8$ films.

Accurate measurements of the electrical properties can provide scientists and engineers with valuable information to properly incorporate the material into its intended applications for more solid design or to monitor a manufacturing process for improved quality control. Therefore, we examine the effect of substrate temperature on the electrical properties of $As_{46}Te_{46}S_8$ films. X-ray diffraction and selected-area electron diffraction (SAED) patterns were used to detect the amorphous and crystalline phases of the films deposited at different substrate temperatures. The film thickness dependence of the optical band gap (E_0), the high-frequency dielectric constant (ε_∞) and the carrier concentration (N) was also studied.

2. Experimental details

Bulk $As_{46}Te_{46}S_8$ chalcogenide glass was prepared using the standard melt-quenching technique [22, 23]. High-purity (99.999%) As, Te, and S in appropriate atomic weight percentages were weighed and sealed in a quartz ampoule (12 mm diameter) under a vacuum pressure of 10^{-4} Torr. The content was heated at approximately 1100 K for 24 hours. During the melting process, the tube was frequently shaken to homogenise the resulting alloy. The melt was quenched in ice water to obtain the glassy state. The content of the alloy was verified by energy dispersive X-ray spectroscopy (EDX) using a scanning electron microscope (Shimadzu Superscan SSX-550).

The thin films were prepared via thermal evaporation onto chemically cleaned glass substrates using an Edwards E306 coating unit operated at 10^{-5} Torr. Direct thermal evaporation was performed from a small quartz crucible, which was heated using a conical basket of tungsten wire as a filament. Evaporation was initiated by passing a low current in the filament for a period sufficient to heat up the material. The current was gradually and carefully increased, and when the material melted inside the crucible, the current was increased fairly rapidly to avoid alloy decomposition. The films were deposited at different substrate temperatures ranging from room temperature to 458 K. The substrate was heated using an accessory consisting of a sheathed heater coil, reflector and spherical work holder, a thermocouple (Cu-constantan), lead through and a meter to indicate and regulate the substrate temperatures. The mechanical rotation of the glass substrate holder facilitated the deposition of homogenous films at a high deposition rate of 10 nm/s.

The elemental composition (As, Te, and S) of the investigated $As_{46}Te_{46}S_8$ films was determined using EDX at different locations on the sample, and the average values were recorded. The film thicknesses, in the range of 35 - 135 nm, were measured using a quartz crystal thickness monitor (FTMS, Edwards, UK) [24]. The earthed face of the crystal monitor was facing the source and was placed at the same height as the substrate. The margin of error in the obtained thickness was $\pm$ 0.05%.

Differential scanning calorimetry (DSC) was performed using a Shimadzu TA-50 (Japan) instrument at a heating rate of 25 K/min. X-ray investigations were performed using a Philips diffractometer type 1710 with a Ni-filtered $Cu\ K\alpha$ source (λ =0.154 nm) at 40 kV and 30 mA with a scanning speed of 3.5°/min. The structure of the film deposited at different substrate

temperatures was analysed using a JEOL2000 transmission electron microscope (TEM) operated at 100 kV.

The optical absorption and transmission data were obtained using a computerised UV-2101 double-beam spectrophotometer in the wavelength range of 300-900 nm. The electrical conductivity measurements were performed in the dark over the temperature range of 300-420 K for films with evaporated gold electrodes using a Tohr cryogenic cryostat. A conventional circuit using a Keithley 610C electrometer was used for the electrical measurements.

3. Results & Discussion

3.1. Structure

A DSC thermogram was obtained for a bulk glass sample of 16.4 mg using a heating rate of 25 K min^{-1}. The glass transition and the peak crystallisation temperatures were 396 K and 488 K, respectively, as indicated in Fig. 1.

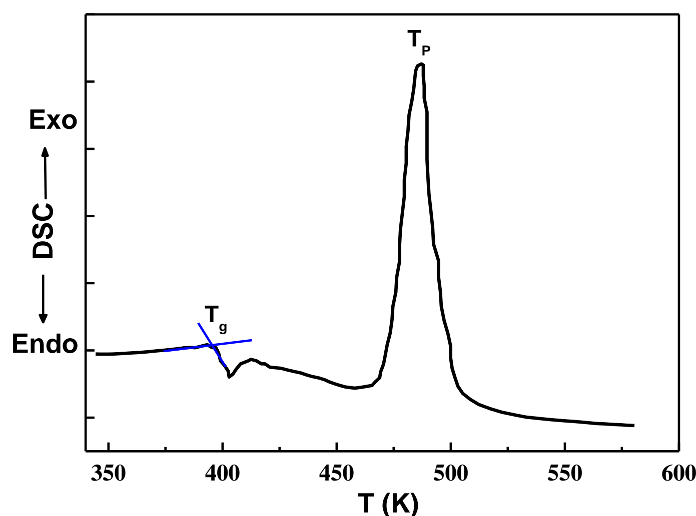

Fig. 1. DSC thermogram obtained for a bulk glass sample at a rate of 20 K min^{-1}.

The X-ray diffraction patterns of the $As_{46}Te_{46}S_8$ films deposited at substrate temperatures T_S of room temperature, 413 K, and 458 K are presented in Fig. 2. It is clear that the film deposited at T_S = room temperature has a typical amorphous structure. For the substrate deposition temperatures T_S= 413 and 458 K, different crystalline peaks (phases) can be identified. These crystalline phases correspond to As_2Te_3, AsTe, and AsS. No ternary phases are observed, possibly because of the consumption of the relatively small amount of S in forming the AsS binary phases.

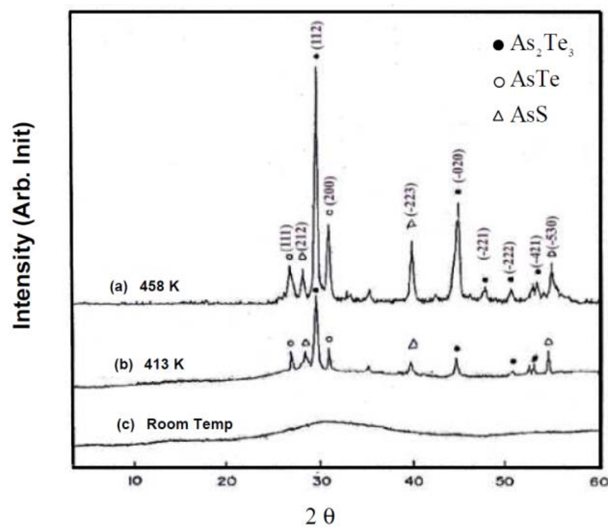

Fig. 2. X-ray diffraction pattern of $As_{46}Te_{46}S_8$ films deposited at different substrate temperatures.

The selected-area electron diffraction (SAED) patterns of the films deposited at different substrate temperatures are presented in Fig. 3. The diffuse rings in the electron diffraction pattern (Fig. 3a) indicate the amorphous phases of the film deposited at T_S = room temperature.

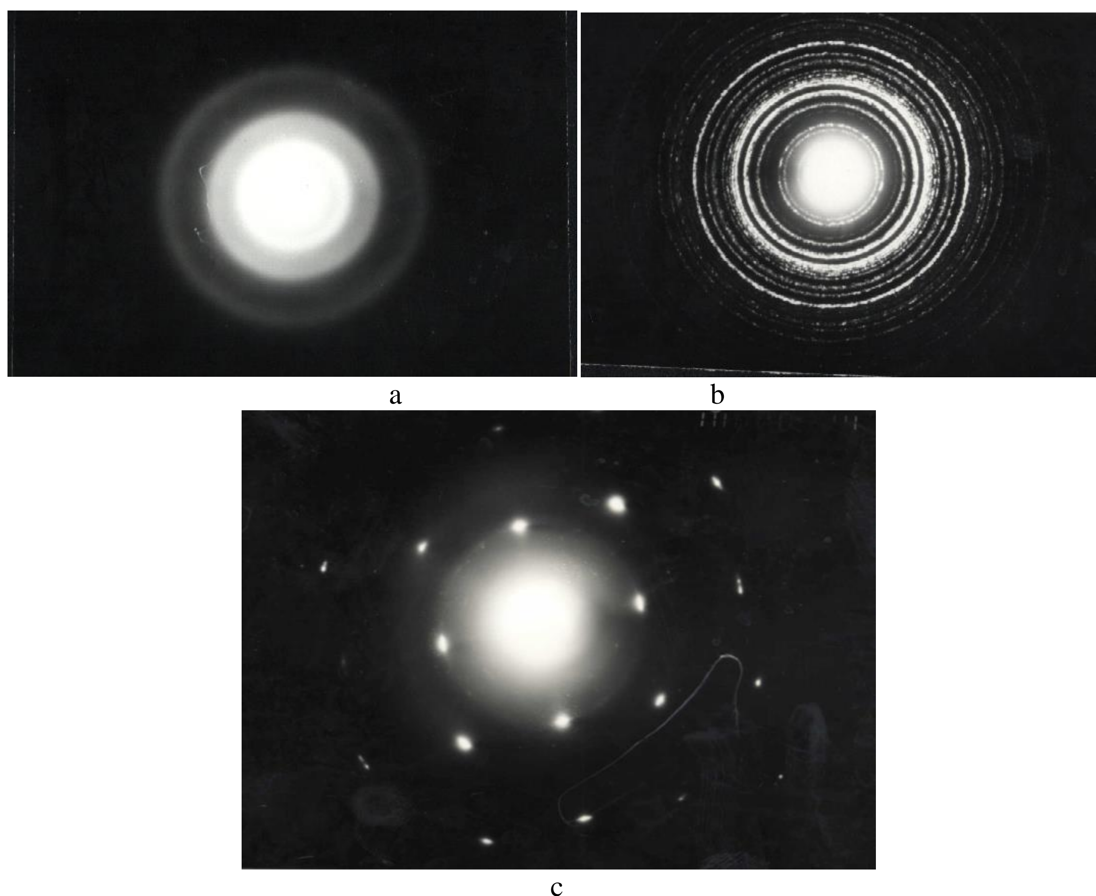

Fig. 3. The selected-area electron diffraction patterns of films deposited at different substrate temperatures, T_S: (a) T_S=R.T., (b) T_S= 413 K, (c) T_S= 458 K.

Sharp diffraction rings appeared in the electron diffraction pattern for the film deposited at T_S =413 K (Fig. 3b). Analysis of the SAED patterns determines the most probable crystalline phases accompanying the transformations. To index the planes in the electron diffraction patterns, the d-spacing corresponding to the different radii of the diffraction patterns of the deposited films must be determined. The d-spacing was calculated using the relation $d = \lambda L / R$, where R is the radius of the diffuse rings and L is the camera length, which represents the distance between the specimen and the photographic film. λL is called the camera constant and can be determined using a standard specimen (Au film) to record the diffraction pattern. Thus, the radius (R) was measured on the negative substitute on the gold diffraction standard. Using the calculated d-spacing of the films deposited at T_S = 413 K (Fig. 3b), the planes of the diffraction patterns are indexed as (112), (200), and (-223) using ASTM cards; these values correspond to the crystallisation phases As_2Te_3, AsTe, and AsS, respectively. These results were confirmed by the results of the X-ray diffraction investigation.

Fig. 3c presents the spot pattern for the film deposited at T_S = 458 K. The spots are not indexed, which means that single crystal phases occurred at this substrate deposition temperature.

3. 2. Effect of film thickness and substrate temperature on the optical properties

The important applications of chalcogenide glasses, such as optical recording materials and, more recently, diffractive optics and optical integrated circuits for IR operations, require the fabrication of structures in a range of film thicknesses from one to a tenth of a micron [25]. The variation in the optical energy gap as a function of substrate temperature may provide deeper insight into the mechanisms of disorder and defect formation in amorphous chalcogenides [26].

A study of the optical constant in the vicinity of the absorption edge yielded significant information on the role of various atoms in the chalcogenide network. It is known that if the multiple reflections are neglected, the transmittance (T) of perfectly smooth deposited films and substrates is given by the following relation [27]:

$$T = (1-R)^2 e^{(-A)} = (1-R)^2 e^{(-\alpha d)}, \tag{1}$$

where R is the reflectance, A is the absorption, α is the absorption coefficient in cm^{-1} and d is the film thickness in cm. This expression can be successfully applied to calculate α using the following relation:

$$\alpha = \frac{1}{d} \ln[(1-R)^2 / T]. \tag{2}$$

To describe light absorption by media, the extinction coefficient $k = \alpha\lambda / 4\pi$ can be introduced. The reflectance of a material of refractive index (n) is given by

$$R = \frac{(n-1)^2 + k^2}{(n+1)^2 + k^2}, \tag{3}$$

The refractive index (n) can be determined from Eq. (3) using the following relation:

$$n = \frac{(1+R)}{(1-R)} \pm \sqrt{(\frac{R+1}{R-1})^2 - (1+k^2)}, \tag{4}$$

In our work, a realistic value of n was determined by considering the plus sign in Eq. (4).

In crystalline semiconducting materials, electronic transitions occur between the highest energy of the valence band and the lowest energy of the conduction band. When the extremes have the same momentum vector value (k), the transition is direct. Otherwise, only phonon-assisted transitions are possible, which are called indirect transitions [28, 29].

3.2.1. Effect of the film thickness on the optical band gap

The optical absorption spectrum in amorphous semiconductors has been observed to have three distinct regions [30]: the weak absorption tail, which originates from defects and impurities; the exponential edge region, which is strongly related to the structural randomness of the system; and the high absorption region, which determines the optical energy gap. In the high absorption region ($\alpha > 10^4$ cm^{-1}), a parabolic relation can be applied:

$$\alpha h\nu = B\,(h\nu - E_0)^r\,, \tag{5}$$

where h is Plank's constant, ν is the frequency, E_0 is the optical energy gap of the investigated film, and r is an index that has values of 2, 3, 1/2, and 3/2 depending on the nature of the electronic transition responsible for the absorption [13, 30].

The usual method for determining the value E_0 involves plotting a graph of $(\alpha h\nu)^r$ vs. photon energy ($h\nu$). If an appropriate value of r is used to linearise the graph, the value of E_0 will be given by the intercept on the $h\nu$-axis. The results in the present experiment (Fig. 4) for $As_{46}Te_{46}S_8$ thin films deposited at T_S = room temperature at two different thicknesses, as representative cases, obey Eq. (5) with r = 1/2. This result indicates that a direct transition is the most probable mechanism. The values of E_0 calculated from Fig. 4 at different thicknesses are listed in Table 1. Fig. 5 demonstrates the dependence of E_0 on the film thickness: E_0 increases with increasing thickness up to 70 nm and then becomes constant as the film thickness continues to increase. Thus, the film thickness does not appreciably affect E_0 in the film thicknesses range of 70-135 nm.

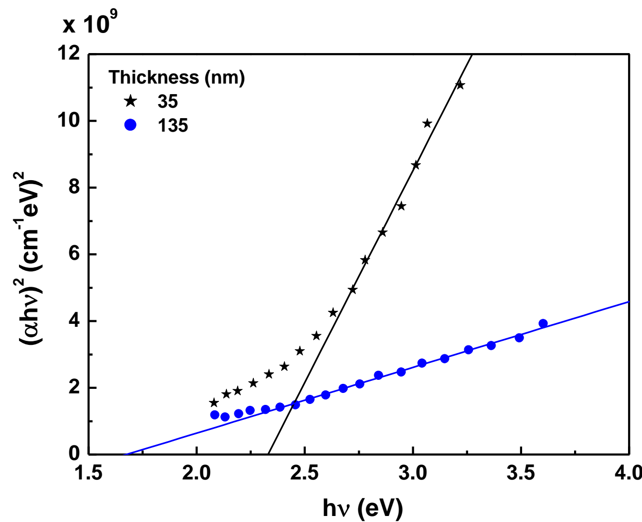

Fig. 4. Variation of $(\alpha h\nu)^2$ with the photon energy $h\nu$ at two film thicknesses.

Table 1. The dependence of the direct optical energy gap $\left(E_0\right)$, the high frequency dielectric constant $\left(\varepsilon_\infty\right)$, and the ratio $\left(N / m^*\right)$ on the thickness of $As_{46}Te_{46}S_8$ films deposited at T_S = room temperature.

Thickness (nm)	E_0 (eV)	ε_∞	$\left(N / m^*\right)\times10^{22}$ $\left(\text{cm}^{-3}\right)$
35	1.70	14.36	1.23
45	2.04	19.18	1.56
54	2.19	23.43	1.78
63	2.24	27.43	1.89
75	2.33	27.62	1.90
90	2.34	29.91	2.12
117	2.37	33.88	2.79
135	2.37	35.73	3.34

The result of an increase in the optical band with increasing film thickness is in good agreement with the results observed for many chalcogenide thin films [22, 31-34] and can be interpreted based on the model of the density of states in amorphous solids proposed by Mott and Davis [35] by assuming the presence of defects in the amorphous thin film. During the deposition of an amorphous film, unsaturated bonds are proposed to exist because of an insufficient number of atoms [36]. The unsaturated bonds are responsible for the formation of some defects in the film. Such defects produce localised states in the amorphous solids. For a thicker film, greater depositions generate a more homogeneous network by saturating the dangling bonds and thereby minimising the number of defects. Thus, the concentrations of localised states are reduced, and the optical band gap consequently increases. Thus, thicker films with a lower concentration of dangling bonds should have larger optical gaps than thinner ones.

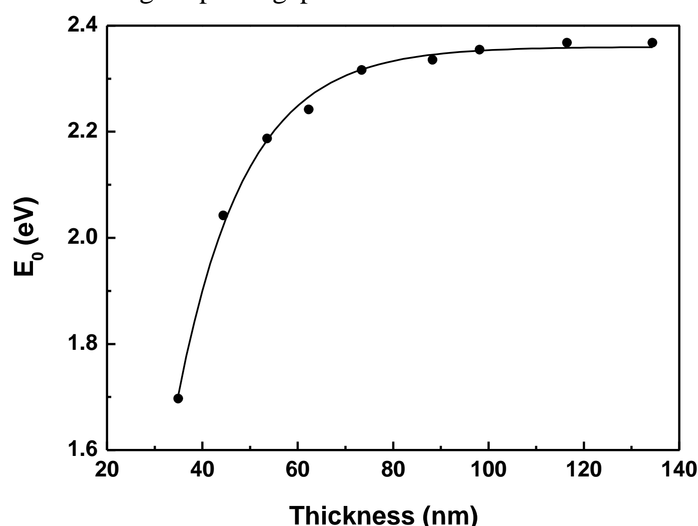

Fig. 5. The dependence the optical energy gap, E_0, of the investigated films on film thickness.

3.2.2. Effect of film thickness on the high-frequency dielectric constant and carrier concentration

Any absorbing medium can be characterised by the complex refractive index $\left(\tilde{n} = n - ik\right)$ and the complex dielectric constant or the relative permittivity $\left(\varepsilon = \varepsilon_1 - i\,\varepsilon_2\right)$. The complex dielectric constant of media varies depending on the photon energy or angular

frequency of the incident light [37]. When the real component of the real permittivity ε_1 is quite low, the value of ε_1 is represented by the static dielectric constant ε_S, which includes the contributions of both atomic and electrical polarisations [37]. Furthermore, when the photon energy is higher than that in the infrared region, the atomic polarisation disappears; consequently, the ε_1 value decreases to the value of the high-frequency dielectric constant ε_∞. In semiconductor crystals, such as InAs, ZnTe, and ZnS, ε_∞ decreases almost linearly as the band gap increases [38].

To better understand the optical properties of the investigated film, it is necessary to determine some of the optical constants, such as the high-frequency dielectric constant ε_∞ and the carrier concentration *N*. The real component of the relative permittivity ε_1 and the squares of the wavelength (λ^2) are related by the following equation [39, 40]:

$$\varepsilon_1 = n^2 = (1+\sqrt{R})^2 / \left(1-\sqrt{R}\right)^2 = \varepsilon_\infty - \left(\frac{e^2}{\pi C^2}\right)\left(\frac{N}{m^*}\right)\lambda^2, \qquad (6)$$

where *C* is the velocity of light, *e* is the electronic charge and m^* is the electron effective mass. According to Eq. (6), the high-frequency dielectric constant ε_∞ and the ratio $\left(N/m^*\right)$ of the investigated films deposited at different thicknesses can be determined from the linear plot of ε_1 vs. λ^2, as shown in Fig. 6. The calculated values of ε_∞ and N/m^* are listed in Table 1; the values of ε_∞ and $\left(N/m^*\right)$ increase with increasing film thickness. In other words, these values increase as the saturation of dangling bonds increases, which indicate that these parameters are related to the internal microstructure of the film. As observed in Fig. 6, the refractive index increases with increasing film thickness for $\lambda < 600$ nm. Furthermore, the refractive index for film thicknesses greater than 75 nm is independent of the thickness. These results are also in agreement with those obtained for other chalcogenide glasses [31] and may be attributed to the discontinuity of the film in the initial deposition stages.

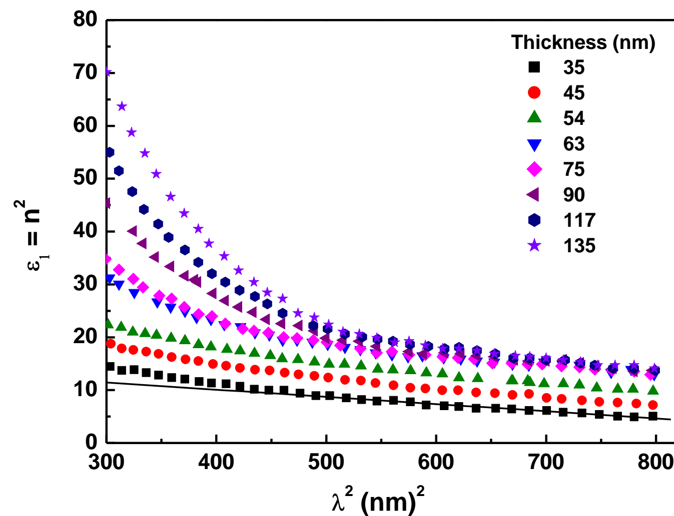

Fig. 6. The variation of $\varepsilon_1 = n^2$ *with the square of the wavelength* λ^2 *for different film thicknesses.*

3.2.3. Effect of substrate temperature on the optical band gap

Thin films of the same thickness (d = 100 nm) were deposited on substrates held at different temperatures in the range of 300-463 K. A good fit between the experimental points of the spectral dependence of the absorption coefficient with the straight $(\alpha h\nu)^2$ vs. $(h\nu)$ lines can be observed in Fig. 7. This fit confirms that a direct transition of the electrons is the predominate absorption mechanism in the $As_{46}Te_{46}S_8$ films. The values of E_0, calculated from the intercepts of the $(\alpha h\nu)^2$ vs. $(h\nu)$ plots in Fig. 7, are plotted as a function of T_S in Fig. 8 and are presented in Table 2. It is clear that E_0 increases with increasing T_S in the temperature range of 363-463 K. The increase in the band gap energy with increasing substrate temperature can be attributed to a shift in stoichiometry which was encountered in the previous work [41].

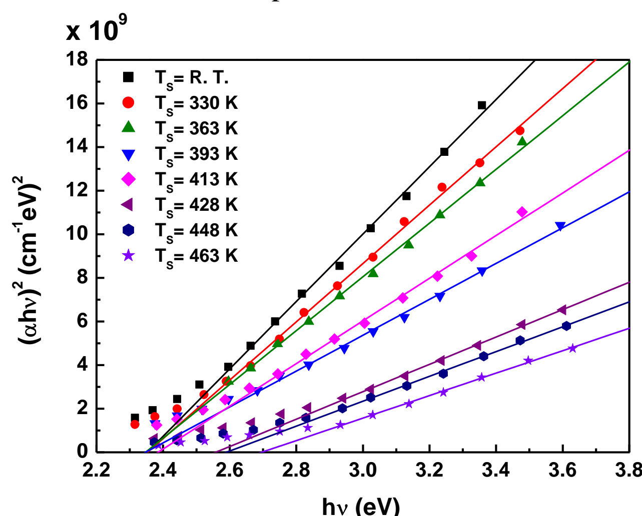

Fig. 7. Variation of $(\alpha h\nu)^2$ with photon energy $h\nu$ at different substrate temperatures.

In the exponential edge region ($1 < \alpha < 10^4$ cm^{-1}), the band tail width, E_e, which represents the degree of disorder in amorphous semiconductors, can be determined from the following relation [42]:

$$\alpha = \alpha_0 \exp(h\nu / E_e), \tag{7}$$

where $h\nu$ is the photon energy and α_0 is a constant. The spectral dependence of the absorption coefficient of the $As_{46}Te_{46}S_8$ films (d=100 nm) deposited at T_S = room temperature and 428 K, as representative cases, is presented in Fig. 9. Generally, the absorption coefficient (α) decreases with increasing substrate temperature. The calculated values of the band tail width, E_e, at different substrate temperatures were already presented in Fig. 8 and listed in Table 2.

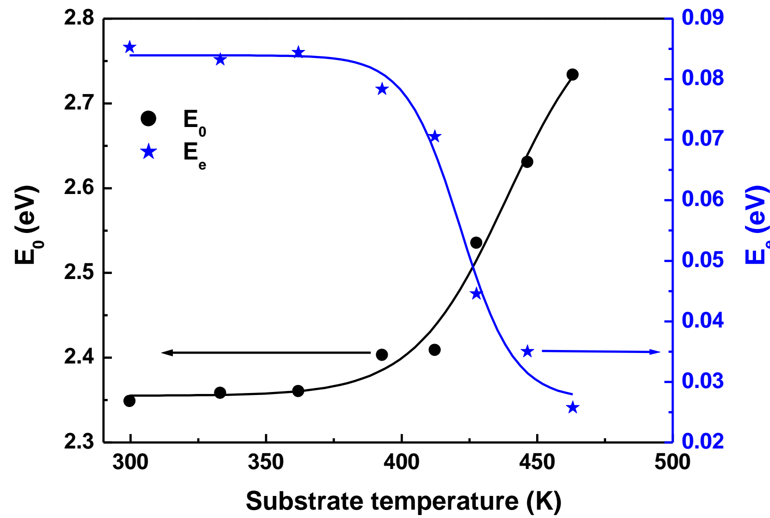

Fig. 8. Variation of the optical energy gap, E_0, and the band tail width, E_e, as a function of substrate temperature

Table 2. The activation energy gap (ΔE) for conduction, the resistivity (ρ), Optical energy gap (E_0), and the band tail width (E_e) for $As_{46}Te_{46}S_8$ films deposited at different substrate temperature T_S (d = 100 nm).

Substrate Temperature (K)	ΔE (eV)	ρ (Ω cm)	E_0 (eV)	E_e (eV)
R. T.	0.55	$7.74x\ 10^5$	2.35	0.085
330	0.52	$5.98x\ 10^5$	2.36	0.083
363	0.47	$3.16x\ 10^5$	2.36	0.084
393	0.41	$1.14x\ 10^5$	2.40	0.078
313	0.22	$1.89x\ 10^3$	2.41	0.070
428	0.18	$1.14x\ 10^3$	2.54	0.044
448	0.15	$6.81x\ 10^2$	2.63	0.034
463	______	______	2.73	0.025

An increase in E_0 as E_e decreases and T_S increases is also observed. This behaviour could also be interpreted based on the Mott and Davis model [35]. According to this model, the width of the localised states near the mobility edges depends on the degree of disorder and defects, which depend upon the unsaturated bonds produced during deposition [35]. At higher values of the substrate deposition temperature, an unsaturated bond gains sufficient energy for rearrangement during the formation of the film, producing a large number of saturated bonds. This process, in turn, reduces the density of localised states, re-distributes the atomic distance and bond angle and, consequently, decreases E_e. Thus, the substrate temperature dependence of E_e reflects the presence of defects and the degree of disorder of amorphous thin films. This interpretation confirmed the observed increase in E_0 with increasing T_S resulting from the amorphous to crystalline transformation, followed by the increase of the ratio of crystalline phases in the film [43-45], as observed in the structural investigation of figures 1, 2 and 3.

However, the decreasing of the absorption coefficient with increasing substrate temperature (Fig. 9) can be explained based on the change in the nature of the film at it transitions from the amorphous to the crystalline state. The XRD patterns in Fig. 2 indicated that the diffraction peaks strongly increased as the substrate temperature increased from 413 to 458 K, which revealed the formation of more crystallites. A similar trend was reported [46] previously for other films deposited on heated glass substrates, which means that the optical transmittance (T) of

the film increases and consequently, according to equation (2), the absorption coefficient decreases with increasing substrate temperature.

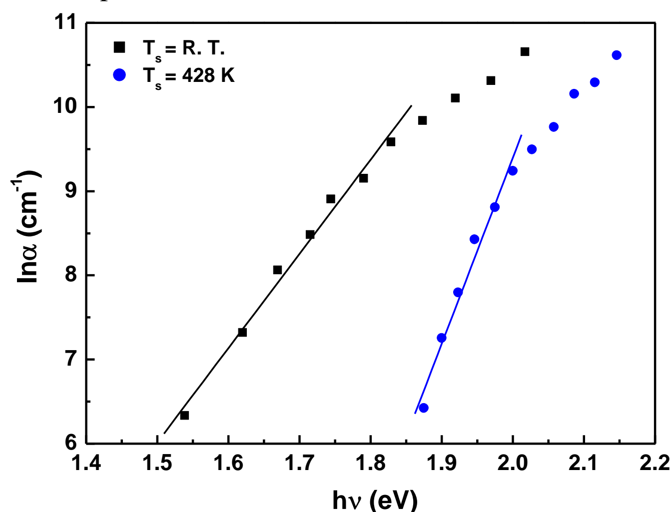

Fig. 9. Variation of ln α with photon energy hν at two different substrate temperatures.

3.3 Effect of substrate temperature on the electrical properties

The effect of substrate temperature on the electrical resistivity, ρ, and activation energy for conduction, ΔE, of the $As_{46}Te_{46}S_8$ films was studied. For this purpose, 100-nm-thick films were deposited onto glass substrates held at different temperatures in the range of 300-443 K. Electrical resistivity measurements of the films were performed using evaporated gold electrodes.

The resistivity values varied with temperature according to an Arrhenius relation [12, 13]:

$$\rho = \rho_0 \exp(-\Delta E / k_B T), \quad (8)$$

where k_B is the Boltzmann constant and ρ_0 is the pre-exponential factor of resistivity. The activation energy for electrical, ΔE , is a function of the electronic energy levels of the atoms in the amorphous material and hence of the emerging band gap. Fig. 10 presents log ρ vs. $1/T$ plots for films (d = 100 nm) deposited at different substrate temperatures. According to Eq. (8), one can establish that the electrical behaviour of $As_{46}Te_{46}S_8$ films at low voltages (where Ohm's law is valid) is characteristic of intrinsic semiconductors. Therefore, the electrical conduction is primarily due to excited carriers in the extended states belonging to the conduction band of the glassy semiconductor [35]. The values of ρ and ΔE, which were calculated from Fig. 10, are presented in Table 2.

The value of ΔE for the film deposited on a substrate held at room temperature (≈ 0.55 eV; Table 2) is very close to that reported for a narrow-band semiconductor [47]. The increase in the conductivity and the decrease in ΔE upon increasing T_S (Table 2) may be attributed to the amorphous-crystalline transformations. Thus, the substrate temperature dependence of the activation energy for conduction and electrical conductivity is consistent with the interpretation of the optical data.

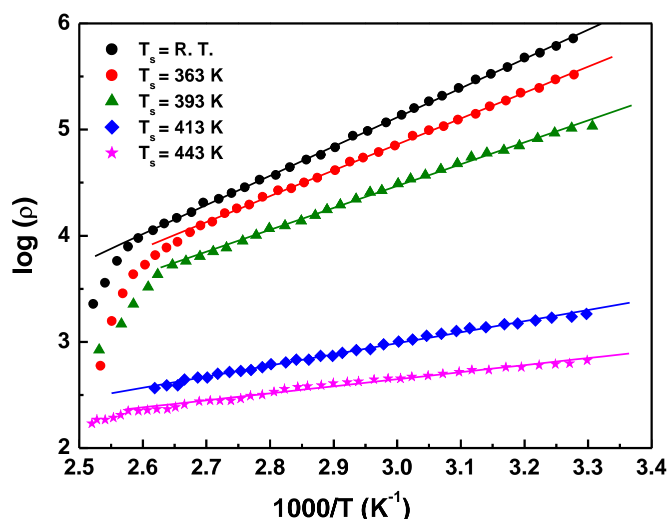

Fig. 10. Log ρ vs. 1/T for films (d = 100 nm) deposited at different substrate temperatures.

4. Conclusions

XRD and TEM investigations of $As_{46}Te_{46}S_8$ revealed that the film deposited onto a substrate at room temperature had a typical amorphous structure, while several crystalline peaks were observed for the films deposited at T_S = 413 and 458 K.

The optical data for $As_{46}Te_{46}S_8$ indicated that the electronic transition responsible for the optical absorption occurred through a direct transition process. The parameters E_0, ε_∞ and N/m^* are affected by the film thickness. This result confirms the effect of the film thickness on the density of localised states and microstructure of the studied samples.

It is reasonable to assume that the observed changes in the optical properties with substrate temperature resulted from the microstructure rearrangement initiated during deposition, which implies that a higher temperature creates a more homogenous network and minimises the number of defects.

Due to the amorphous-crystalline transformations, both the electrical resistivity and the activation for conduction decreased with increasing substrate temperature.

The corresponding increase in the optical constants such as refractive index and high frequency dielectric constant with increasing film thickness is correlated with increase in the density of defect states.

References

[1] D Singh, S Kumar, R Thangaraj and T S Sathiaraj Physica B **408** 119 (2013)
[2] Z R Khan, M Zulfequar and M S Khan Chalcogenide Lett. **7** 431 (2010)
[3] S Sen, E L Gjersing and B G Aitken J. Non-Cryst. Solids **356** 2083 (2010)
[4] B Bureau, S Danto, H L Ma, C Boussard-Pledel, X H Zhang and J Lucas Solid State Sci. **10** 427 (2008)
[5] M H R Lankhorst, B W S M M Kerelaars and R A M Wolter Nat. Mater. **4** 347 (2005)
[6] A Zakery and S R Ellilott J. Non-Cryst. Solids **330** 1 (2003)
[7] P J S Ewen Photo-induced Metastability in Amorphous Semiconductors (Germany: Wiley-VCH, Weinheim) (ed) A V Kolobov 365 (2003)
[8] K Nandakumar and J Philip J. Non-Cryst. Solids **144** 247 (1992)
[9] E Marquez, J M Gonzalez-Leal, R Prieto-Alcon, M Vlcek, A Stronski, T Wagner, D Minkov Appl. Phys. A **67** 371 (1998)
[10] A H Moharram Appl. Phys. A **66** 77 (1998)

[11] M Ohto, M Itoh and K Tanaka J. Appl. Phys. **77** 1034 (1995)
[12] A M Ahmed, M M Wakkad, S H Mohamed and A K Diab Indian J Phys **87** 317 (2013)
[13] A H Ammar, M S Abo Ghazala, A A M Farag and A Eleskandrany Indian J Phys **87** 1169 (2013)
[14] A Alegria, A Arruabarrena and F Sanz J. Non-Cryst. Solids **58** 17 (1983)
[15] D P Gasain, T Shimizu, M Ohmura, M Suzuki, T Bando and S Okano J. Mater. Sci. **26** 3271 (1991)
[16] H W Pinsler and W E Brower J. Phys. Chem. Sol. **38** 393 (1977)
[17] D R Uhlamann and N I Kreidl Glass forming systems, Glass Science and Technology, Vol. 1 (USA, New York: Academic Press) 241 (1983)
[18] R Naik, C Kumar, R Ganesan and K S Sangunni Mater. Chem. Phys. **130** 750 (2011)
[19] J Cornet and D Rossier J. Non-Cryst. Solids **12** 85 (1973)
[20] Q Ma, D Raoux and S Benazeth J. Non-Cryst. Solids **150** 366 (1992)
[21] M Tenhover, P Boolchand and W J Bresser Phys. Rev. B **27** 7533 (1983)
[22] A A Joraid, S N Alamri, A S Solieman and A A Abu-Sehly Opt. Laser Technol. **43** 1243 (2011)
[23] A S Soltan, A A Abu-Sehly, A A Joraid and S N Alamri Thermochim. Acta **574** 73 (2013)
[24] A S Soltan Appl. Phys. A **80** 117 (2005)
[25] E Marquez, J M Gonzalez-Leal, A M Bernal-Olive, R Jimenez-Garay and T Wanger J. Non-Cryst. Solids **354** 503 (2008)
[26] M M El–Samanoudy and M Fadel J. Mat. Sci. **27** 646 (1992)
[27] T S Moss Optical properties of Semiconductor (New York: Academic Press) 19 (1959)
[28] E A Davis and N F Mott Phill. Mag. **22** 903 (1970)
[29] H Frizsche J. Non-Cryst. Solids **6** 49 (1971)
[30] J Taus Amorphous and Liquid Semiconductors (New York: Plenum Press) 159 (1974)
[31] E Kh Shokr and M M Wokkad J. Mater. Sci. **27** 1197 (1992)
[32] A A Abu-Sehly and M I Abd-Elrahaman J. Phys. Chem. Solids. **63** 163 (2002)
[33] S K Biswas, S Choudhury and A Choudhury Phys. Stat. Sol. **105** 467 (1988)
[34] H T El-Shair and E Bekheet J. Phys. D: Appl. Phys. **25** 1122 (1992)
[35] N F Mott and E A Davis Philosophical Magazine **22** 903 (1970)
[36] S R Ovshinsky and D Adler Contem. Phys. **19** 109 (1978)
[37] H Fujiwara Spectroscopic Ellipsometry principles and applications (England, Chichester: John Wiley and Sons Ltd.) 48 (2007)
[38] S Adachi J. Appl. Phys. **53** 8775 (1982)
[39] H Mahfoz Kotb, M A Dabban, A Y Abdel-Latif and M M Hafiz J. Alloys Comp. **512** 115 (2012)
[40] M M Wakkad J. Phys. Chem. Solids **51** 1171 (1990)
[41] E Bacakiz, S Aksu, I Polat, S Yilmaz and M Altunbas J. Alloys Comp. **487** 280 (2009)
[42] F Urbach Phys. Rev. **92** 1324 (1953)
[43] S M Baker, S C Baylisc, S I Gurman, N Elgun, J S Bates and E A Davis J. Phys. Condens. Matter. **5** 519 (1993)
[44] M Kanzari and B Rezig Semicond. Sci. Technol. **15** 335 (2000)
[45] M Chhowalla et al J. Appl. Phys. **81** 139 (1997)
[16] R Mariappan, V Ponnuswamy and M Ragavendar Materials Sci. in Semiconductor Processing **15** 199 (2012)
[47] P D Ankrumm Semiconductor Electronics (India: Prentic-Hall) 415 (1971)